Original Article | Neuroimaging and Head & Neck

http://dx.doi.org/10.3348/kjr.2013.14.4.662
pISSN 1229-6929 · eISSN 2005-8330
Korean J Radiol 2013;14(4):662-672

Korean Journal of Radiology
KJR

True Progression versus Pseudoprogression in the Treatment of Glioblastomas: A Comparison Study of Normalized Cerebral Blood Volume and Apparent Diffusion Coefficient by Histogram Analysis

Yong Sub Song, MD[1], Seung Hong Choi, MD, PhD[1], Chul-Kee Park, MD[2], Kyung Sik Yi, MD[1], Woong Jae Lee, MD[1], Tae Jin Yun, MD[1], Tae Min Kim, MD[3], Se-Hoon Lee, MD, PhD[3], Ji-Hoon Kim, MD[1], Chul-Ho Sohn, MD[1], Sung-Hye Park, MD[4], Il Han Kim, MD[5], Geon-Ho Jahng, PhD[6], Kee-Hyun Chang, MD[1]

Departments of [1]Radiology, [2]Neurosurgery, [3]Internal Medicine, [4]Pathology and [5]Radiation Oncology, Seoul National University College of Medicine, Seoul 110-744, Korea; [6]Department of Radiology, School of Medicine of Kyung Hee University, Seoul 134-727, Korea

Objective: The purpose of this study was to differentiate true progression from pseudoprogression of glioblastomas treated with concurrent chemoradiotherapy (CCRT) with temozolomide (TMZ) by using histogram analysis of apparent diffusion coefficient (ADC) and normalized cerebral blood volume (nCBV) maps.

Materials and Methods: Twenty patients with histopathologically proven glioblastoma who had received CCRT with TMZ underwent perfusion-weighted imaging and diffusion-weighted imaging (b = 0, 1000 sec/mm^2). The corresponding nCBV and ADC maps for the newly visible, entirely enhancing lesions were calculated after the completion of CCRT with TMZ. Two observers independently measured the histogram parameters of the nCBV and ADC maps. The histogram parameters between the true progression group (n = 10) and the pseudoprogression group (n = 10) were compared by use of an unpaired Student's *t* test and subsequent multivariable stepwise logistic regression analysis to determine the best predictors for the differential diagnosis between the two groups. Receiver operating characteristic analysis was employed to determine the best cutoff values for the histogram parameters that proved to be significant predictors for differentiating true progression from pseudoprogression. Intraclass correlation coefficient was used to determine the level of inter-observer reliability for the histogram parameters.

Results: The 5th percentile value (C5) of the cumulative ADC histograms was a significant predictor for the differential diagnosis between true progression and pseudoprogression (p = 0.044 for observer 1; p = 0.011 for observer 2). Optimal cutoff values of 892 x 10^{-6} mm^2/sec for observer 1 and 907 x 10^{-6} mm^2/sec for observer 2 could help differentiate between the two groups with a sensitivity of 90% and 80%, respectively, a specificity of 90% and 80%, respectively, and an area under the curve of 0.880 and 0.840, respectively. There was no other significant differentiating parameter on the nCBV histograms. Inter-observer reliability was excellent or good for all histogram parameters (intraclass correlation coefficient range: 0.70-0.99).

Conclusion: The C5 of the cumulative ADC histogram can be a promising parameter for the differentiation of true progression from pseudoprogression of newly visible, entirely enhancing lesions after CCRT with TMZ for glioblastomas.

Index terms: *Apparent diffusion coefficient; Cerebral blood volume; Glioblastoma multiforme; Histogram analysis; Pseudoprogression*

Received December 16, 2012; accepted after revision April 4, 2013.
This study was supported by a grant from the National R&D Program for Cancer Control, Ministry of Health & Welfare, Republic of Korea (1120300) and the Korea Healthcare technology R&D Projects, Ministry for Health, Welfare & Family Affairs (A112028).
Corresponding author: Seung Hong Choi, MD, PhD, Department of Radiology, Seoul National University College of Medicine, 101 Daehak-ro, Jongno-gu, Seoul 110-744, Korea.
• Tel: (822) 2072-2861 • Fax: (822) 743-6385 • E-mail: verocay@snuh.org

Korean Journal of Radiology
KJR

INTRODUCTION

Glioblastoma multiforme (GBM) is the most common primary brain tumor in adults, accounting for approximately one percent of all tumors. Despite the evaluation of multiple treatment approaches, the prognosis for patients with GBM is still extremely poor, with an estimated median survival of 9-18 months (1, 2). Currently, maximal safe tumor resection followed by concurrent chemoradiotherapy (CCRT) with temozolomide (TMZ) and adjuvant TMZ is the standard therapy for patients with GBM (3). Determination of the response to therapy is entirely dependent on the interpretation of magnetic resonance (MR) imaging findings and clinical manifestations. In the criteria published by Macdonald et al. (4) in 1990, radiologic assessments of tumor response and disease progression were primarily based on the enhancing tumor area, and conventional MR imaging has been the best at detecting early treatment-related changes. However, radiologists and clinicians have recently observed the occurrence of progressive MR imaging lesions immediately after the end of CCRT with TMZ, which show spontaneous improvement without further treatment other than adjuvant TMZ. This phenomenon is termed pseudoprogression, and it occurs in 20-30% of the patients (5-8). In cases of true tumor progression, there is no reason to continue adjuvant TMZ; while in cases of pseudoprogression, adjuvant TMZ should be continued (6). Because there are no established imaging findings for the identification of pseudoprogression using conventional contrast-enhanced (CE) MR imaging (9, 10), the Response Assessment in Neuro-Oncology (RANO) criteria for high-grade gliomas were revised. Specifically, the revision states that within the first 12 weeks of completion of radiotherapy, when pseudoprogression is most prevalent, progression can only be determined if the majority of the new enhancement is outside of the radiation field or if there is pathologic confirmation of progressive disease (11).

Several studies have attempted to predict true progression or recurrence by using advanced MR imaging techniques such as perfusion-weighted imaging (PWI) and diffusion-weighted imaging (DWI) (12-19). Moreover, recent studies have shown promising usefulness of histogram analysis of these advanced MR imaging in predicting early treatment response or progression-free survival in patients with high-grade glioma (20-23). However, none of these studies have simultaneously used both PWI and DWI for histogram analysis in the same study population. Furthermore, to the best of our knowledge, there have been no reports regarding the use of a cumulative histogram, which has been reported as a promising tool for differentiating high- from low-grade gliomas (24), for differentiating true progression from pseudoprogression in GBM patients who had received CCRT with TMZ. Therefore, the purpose of this study was to explore the role of histogram analysis of both apparent diffusion coefficient (ADC) and cerebral blood volume (CBV) maps based on newly visible, entirely enhancing lesions in discriminating true progression from pseudoprogression, as well as to evaluate the diagnostic performance of these histogram parameters.

MATERIALS AND METHODS

This retrospective study was approved by our institutional review board. The requirement of an informed consent was waived.

Patient Selection

Sixty-four patients with newly diagnosed GBM who had undergone surgical resection or stereotactic biopsy at our institution between February 2010 and December 2011 were selected from our radiology report database. The inclusion criteria were as follows: the patient 1) had a histopathological diagnosis of GBM without an oligodendroglial component based on the World Health Organization criteria; 2) had undergone baseline MR imaging with contrast enhancement within 24-48 hours after surgery or biopsy before subsequent CCRT with TMZ; 3) underwent CCRT with TMZ after surgery or biopsy; and 4) had undergone the first follow-up 3T MR imaging with DWI at b = 0 and 1000 sec/mm^2 and with dynamic susceptibility contrast (DSC) PWI within two months (mean duration: 22 days, range: 11-34 days) after the end of CCRT. We excluded 41 patients due to the following reasons: 1) poor quality of the MR images; 2) no newly visible enhancing lesion on the first follow-up MR images; 3) a newly visible enhancing lesion that did not fulfill the criteria for measurable disease, which is defined as bidimensionally contrast-enhancing lesions with clearly defined margins by CT or MRI scans, with two perpendicular diameters of at least 10 mm, visible on two or more axial slices that are preferably, at most, 5 mm apart with 0-mm skip (11) on the first follow-up MR images and 4) definite disease progression according to the RANO criteria (11). All 23 included patients received adjuvant TMZ. Additionally, we excluded two patients due to

being lost to follow-up and another patient due to a switch to bevacizumab during adjuvant TMZ before the second follow-up MRI. Finally, a total of 20 patients (10 men and 10 women; age range: 24-68 years; mean age: 50.8 ± 13.5 years) underwent the second follow-up MR imaging with contrast enhancement after 2-6 cycles of adjuvant TMZ (mean interval in days between the end of CCRT and the second follow-up MR imaging: 162 days, range: 46-232 days). We analyzed the changes in the previously enhancing lesions on the second follow-up MR imaging and reviewed the medical records of the patients for the confirmation of true progression (n = 10) or pseudoprogression (n = 10) according to the RANO criteria (Fig. 1) (11).

Image Acquisition

For each patient, the first follow-up MR imaging study after the completion of CCRT was performed with one of the following two 3T MR imaging scanners {Signa Excite (GE Medical Systems, Milwaukee, WI, USA) (n = 6 [true progression = 4 and pseudoprogression = 2]); Verio (Siemens MedicalSolutions, Erlangen, Germany) (n = 14 [true progression = 6 and pseudoprogression = 8])} with an eight-channel head coil. The imaging sequences of the brain included axial spin-echo T1-weighted (T1W) images, fast/turbo spin-echo T2-weighted (T2W) images, fluid-attenuated inversion-recovery (FLAIR) images, DWI, DSC-PWI with gadobutrol (Gadovist, Bayer Schering Pharma, Berlin, Germany), and subsequent CE spin-echo T1W images. The MR imaging parameters were as follows: 558-650/8-20 ms/70-90°/384 x 192-212 (TR/TE/FA/matrix) for spin-echo T1W images; 4500-5160/91-106.3 ms/90-130°/448-640 x 220 (TR/TE/FA/matrix) for fast spin-echo T2W images; and 9000-9900/97-162.9 ms/90-130°/199-220 x 220 (TR/TE/FA/matrix) for FLAIR images. The other parameters for the three images were as follows: section thickness, 5 mm with a 1 mm gap and field of view (FOV) of 240 x 240 mm.

Diffusion-weighted imaging was performed with a single-shot spin-echo echo-planar imaging sequence in the axial plane before the injection of contrast material with a TR/TE of 6900-10000/55-70 ms at b = 0 and 1000 sec/mm^2, 35-

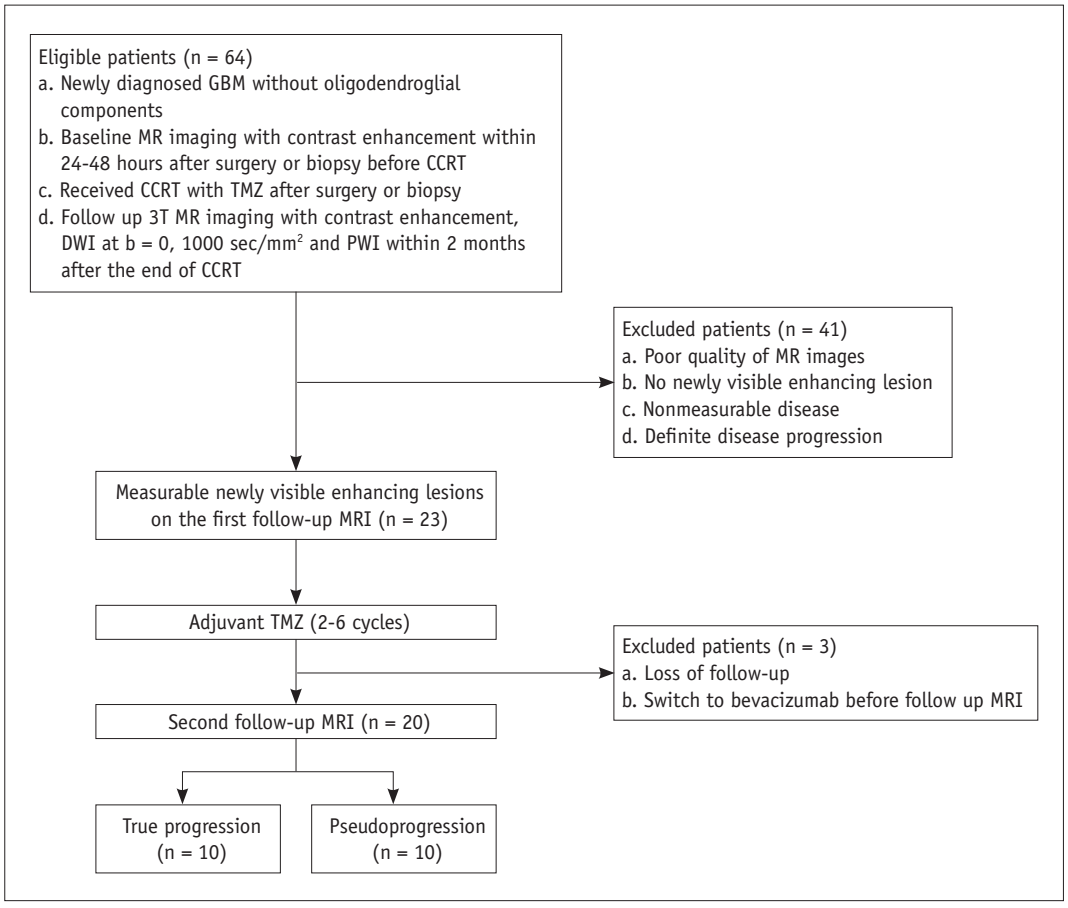

Fig. 1. Flow chart for patient selection and inclusion and exclusion criteria for study. CCRT = concurrent chemoradiotherapy, DWI = diffusion-weighted imaging, GBM = Glioblastoma multiforme, PWI = perfusion-weighted imaging, TMZ = temozolomide

Korean Journal of Radiology
KJR

38 sections, a 3-mm section thickness, a 1-mm intersection gap, an FOV of 240 x 240 mm, a matrix of 160 x 160, three signal averages, and a voxel resolution of 1.5 x 1.5 x 3 mm. DWI data were acquired in three orthogonal directions. Using these data, the averaged ADC maps in the three orthogonal directions were calculated on a voxel-by-voxel basis with the software incorporated into the MR imaging unit.

Dynamic susceptibility contrast-perfusion-weighted imaging was performed with a single-shot gradient-echo echo-planar imaging sequence during the intravenous injection of the contrast agent. The imaging parameters of DSC-PWI were as follows: TR/TE, 1500/30-40 ms; FA, 35-90°; FOV, 240 x 240 mm; 15-20 sections; matrix, 128 x 128; section thickness, 5 mm; intersection gap, 1 mm; and voxel resolution of 1.86 x 1.86 x 5 mm. For each section, 60 images were obtained at intervals equal to the repetition time. After four to five time points, a bolus of gadobutrol at a dose of 0.1 mmol/kg of body weight and at a rate of 4 mL/sec was injected with an MR-compatible power injector (Spectris; Medrad, Pittsburgh, PA, USA). After injecting a bolus of the contrast material, a 30 mL bolus of saline was administered at the same injection rate.

Post-Processing and Histogram Analysis

Histogram analysis was performed using MR imaging data of the first follow-up MR imaging that was performed within two months after the completion of CCRT. The MR imaging data for the conventional MR images, the ADC maps and the DSC-PWI were digitally transferred from the picture archiving and communication system workstation to a personal computer for further analyses. Relative CBV (rCBV) maps were obtained by using a dedicated software package (NordicICE; NordicImagingLab, Bergen, Norway) with an established tracer kinetic model applied to the first-pass data (25, 26). First, realignment was performed to minimize patient motion during the dynamic scanning. Gamma-variate function, which is an approximation of the first-pass response as it would appear in the absence of recirculation, was fitted to the 1/T2* curves to reduce the effects of recirculation. The dynamic curves were mathematically corrected to reduce contrast agent leakage effects (27). After the elimination of recirculation and leakage of contrast agent, the rCBV was computed by means of a numeric integration of the curve. To minimize variances in the rCBV value in an individual patient, the pixel-based rCBV maps were normalized by dividing every rCBV value in a specific section by the rCBV value in the unaffected white matter as defined by a neuroradiologist (S.H.C.) (28). Co-registrations between the CE T1W images and the normalized CBV (nCBV) maps and between the CE T1W images and the ADC maps were performed based on geometric information stored in the respective data sets by using a dedicated software package (NordicICE; NordicImagingLab, Bergen, Norway) (29). The differences in the slice thickness between images were corrected automatically by re-slicing and co-registration method, which was based on underlay images and structural images. The nCBV maps and ADC maps were displayed as color overlays on the CE T1W images.

Two observers (observer 1, a neuroradiologist with eight years of brain MR imaging experience; and observer 2, a neuroradiologist with ten years of brain MR imaging experience), who were blinded to the clinical data, independently compared the CE T1W images that were acquired before the start of the CCRT with those that were acquired after the end of the CCRT. Both the observers then independently drew the regions of interest (ROIs) of the newly visible, entirely enhancing lesions in each section of the co-registered images. Small or thin-rim enhancing lesions that did not fulfill the criteria for measurable disease according to the RANO criteria were not included. Areas of necrosis, cysts, or non-tumor macrovessels that were evident on the CE T1W images were also excluded. The ROI volumes were automatically calculated from the ROIs drawn by each observer. Then, the two observers independently performed histogram analysis in the same manner as described below. The nCBV histograms were plotted with nCBV on the x-axis, with a bin size of 0.1, whereas the y-axis was expressed as a percentage of the total lesion volume by dividing the frequency in each bin by the total number of analyzed voxels. For further quantitative analysis, cumulative nCBV histograms were obtained from the nCBV histograms, in which the cumulative number of observations in all of the bins up to the specified bin was mapped on the y-axis as percentages. The following parameters were derived from the nCBV histograms: 1) the mean, 2) the peak height (PH). In the cumulative nCBV histograms, the 70th, 90th and 95th percentile points (C70, C90 and C95, respectively) were derived (the Xth percentile point is the point at which X% of the voxel values that form the histogram are found to the left of the histogram) (24, 30).

The ADC histograms were plotted with ADC values on the x-axis, with a bin size of 5 x 10^{-5} mm^2/sec, whereas the y-axis was expressed as a percentage of the total lesion

volume by dividing the frequency in each bin by the total number of analyzed voxels. In the same manner as the cumulative nCBV histograms, cumulative ADC histograms were obtained from the ADC histograms. The mean ADC was derived from the ADC histograms. In the cumulative ADC histograms, the 5th percentile point (C5) was also derived (24, 30).

Patient's Clinical Characteristics

We reviewed the patient's clinical characteristics, including age, sex, Karnofsky performance score, history of steroid administration at the time of the first follow-up MR imaging, methylation status of O^6-methylguanine DNA methyltransferase promoter of the tumor, surgery method and radiation dose of the CCRT, to determine whether any of these characteristics were predictors of true progression and pseudoprogression.

Statistical Analysis

All statistical analyses were performed with MedCalc software (Version 11.1.1.0 for Microsoft Windows 2000/XP/Vista/7, MedCalc Software, Mariakerke, Belgium). The results with p values of < 0.05 were considered statistically significant.

Clinical characteristics were compared between the true progression group and the pseudoprogression group using Fisher's exact or chi-square tests for the categorical variables.

Because the non-categorical variables of clinical characteristics and histogram parameters were normally distributed according to the Kolmogorov-Smirnov's test, an unpaired Student's t test was employed to compare these variables between the true progression group and the pseudoprogression group.

Subsequently, multivariable stepwise logistic regression analysis was used to determine the significant predictors for the differential diagnosis between true progression and pseudoprogression. Variables with a p-value of < 0.05 according to the univariate analysis were used as input variables for multivariable stepwise logistic regression analysis, with iterative entry of variables on the basis of test results (p-values of < 0.05). The removal of variables was based on likelihood ratio statistics with a probability of 0.10. Receiver operating characteristic (ROC) analysis was employed to determine the best cutoff values for the histogram parameters that proved to be significant predictors for differentiating true progression from pseudoprogression.

The intraclass correlation coefficient (0.0-0.20, poor; 0.21-0.40, fair; 0.41-0.60, moderate; 0.61-0.80, good; and 0.81-1.00, excellent correlation) was used to determine the level of inter-observer reliability for the ROI volume and the histogram parameters.

RESULTS

Among the patient clinical characteristics, only patient age was significantly higher in the true progression group than in the pseudoprogression group (Table 1). Two patients in the true progression group were being treated

Table 1. Clinical Characteristics

Clinical Characteristics	True Progression	Pseudoprogression	*P*
Total number of patients	n = 10	n = 10	
Age, in yrs	57.1 ± 8.3	44.4 ± 15.1	0.035*
Sex			0.218†
Male	40% (4 of 10)	60% (6 of 10)	
Female	60% (6 of 10)	40% (4 of 10)	
KPS ≥ 70	90% (9 of 10)	100% (10 of 10)	1.000†
Steroid administration	20% (2 of 10)	0% (0 of 10)	0.474†
Surgery			0.325‡
Stereotactic biopsy	10% (1 of 10)	10% (1 of 10)	
STR	0% (0 of 10)	20% (2 of 10)	
GTR	90% (9 of 10)	70% (7 of 10)	
MGMT promoter methylation	70% (6 of 10)	70% (7 of 10)	1.000†
Radiation dose, Gy	57.7 ± 6.7	60.3 ± 1.2	0.249*

Note.— *Difference between two groups was evaluated using unpaired Student's t test, †Difference between two groups was evaluated using Fisher's exact test, ‡Difference between two groups was evaluated using chi-square test. KPS = Karnofsky performance score, STR = subtotal resection, GTR = gross total resection, MGMT = O6-methylguanine DNA methyltransferase

Korean Journal of Radiology
KJR

with steroids at the time of the first follow-up MR imaging (1 mg dexamethasone or 10 mg prednisolone) none of the patients in the pseudoprogression group were being treated with steroids at the time of the first follow-up MR imaging.

Table 2 summarizes the nCBV and ADC histogram parameters in the true progression group and the pseudoprogression group as measured by observers 1 and 2. For observer 1, the C5 of the cumulative ADC histograms (p = 0.009) and the mean ADC (p = 0.023) were significantly lower in the true progression group than in the pseudoprogression group. For observer 2, the C5 of the cumulative ADC histograms (p = 0.009) and the C95 of the cumulative nCBV histograms (p = 0.015) were significantly lower in the true progression group than in the pseudoprogression group. The C5 of the cumulative ADC histogram and the mean ADC measured by observer 1, as well as patient age, were used as input variables for a multivariable stepwise logistic regression analysis. In the multivariate analysis, the C5 of the cumulative ADC histogram was the only independently differentiating variable (p = 0.044) whereas patient age and mean ADC were excluded from the logistic regression equation. Likewise, we used the C5 of the cumulative ADC histogram and the C95 of the cumulative nCBV histogram measured by observer 2, as well as patient age, as input variables for another multivariable stepwise logistic regression analysis. In the multivariate analysis, the C5 of the cumulative ADC histogram was the only independently differentiating variable (p = 0.011) whereas patient age and C95 of the cumulative nCBV histogram were excluded from the logistic regression equation (Figs. 2, 3).

Regarding the C5 values of the cumulative ADC histograms measured by both observers 1 and 2, the cutoff values that provided a balance between sensitivity and specificity for the diagnosis of true progression and pseudoprogression were 892 x 10^{-6} mm^2/sec and 907 x 10^{-6} mm^2/sec, respectively. When newly visible, enhancing lesions after CCRT with TMZ having a C5 value below the determined cutoff values were diagnosed as true progression, the sensitivity, specificity, and area under the ROC curve were 90% (9 of 10 patients, 95% CI: 55.5-99.7%), 90% (9 of 10, 95% CI: 55.5-99.7%), and 0.880 (95% CI: 0.658-0.981), respectively, for observer 1 and 80% (8 of 10 patients, 95% CI: 44.4-97.5%), 80% (8 of 10, 95% CI: 44.4-97.5%), and 0.840 (95% CI: 0.609-0.963), respectively, for observer 2.

Inter-observer reliability was excellent or good for the ROI volume and all histogram parameters (intraclass correlation coefficient for ROI volume, 0.97; for C5 of the cumulative ADC histogram, 0.96; for the mean ADC, 0.96; for C95 of the cumulative nCBV histogram, 0.95; for C90 of the cumulative nCBV histogram, 0.96; for C70 of the cumulative nCBV histogram, 0.92; for PH of the nCBV histogram, 0.70; for the mean nCBV, 0.99).

DISCUSSION

In this study, we used the histogram analysis method to differentiate true progression from pseudoprogression based on the nCBV and ADC of newly visible, entirely enhancing lesions on the first MR imaging that was performed within

Table 2. Normalized Cerebral Blood Volume (nCBV) and Apparent Diffusion Coefficient (ADC) Histogram Parameters in True Progression Group and Pseudoprogression Group

	True Progression (n = 10)		Pseudoprogression (n = 10)		$P^{\dagger}$	
	Observer 1	Observer 2	Observer 1	Observer 2	Observer 1	Observer 2
ROI volume	7.2 ± 5.8	4.8 ± 2.6	13.4 ± 14.2	14.8 ± 14.8	0.213	0.062
ADC						
C5*	826 ± 91	832 ± 108	954 ± 104	958 ± 82	0.009	0.009
Mean*	1249 ± 180	1293 ± 236	1448 ± 178	1433 ± 178	0.023	0.149
nCBV						
C95*	4.157 ± 2.569	3.832 ± 1.742	5.481 ± 1.586	5.874 ± 1.654	0.183	0.015
C90	3.676 ± 2.206	3.402 ± 1.555	4.369 ± 1.322	4.583 ± 1.311	0.405	0.083
C70	2.554 ± 1.164	2.278 ± 0.823	3.035 ± 1.074	3.014 ± 1.101	0.349	0.108
Peak height	1.630 ± 0.788	1.700 ± 1.342	2.060 ± 1.159	2.150 ± 1.209	0.345	0.441
Mean	2.123 ± 0.934	2.184 ± 1.109	2.629 ± 0.815	2.649 ± 0.848	0.214	0.307

Note.— Values are expressed as mean ± standard deviation. C95, C90 and C70 refer to 95th, 90th and 70th percentile points of cumulative nCBV histogram, respectively. ROI volumes are expressed as cubic centimeters (cm^3). ADC (b = 1000 sec/mm^2) measurements are expressed as x 10^{-6} square millimeters per second. C5 refers to 5th percentile point of cumulative ADC histogram (Xth percentile point is point at which X% of voxel values that form histogram are found to left in histogram). *Significant difference between two groups (p < 0.05), †Difference between two groups was evaluated using unpaired Student's t test. ROI = region of interest

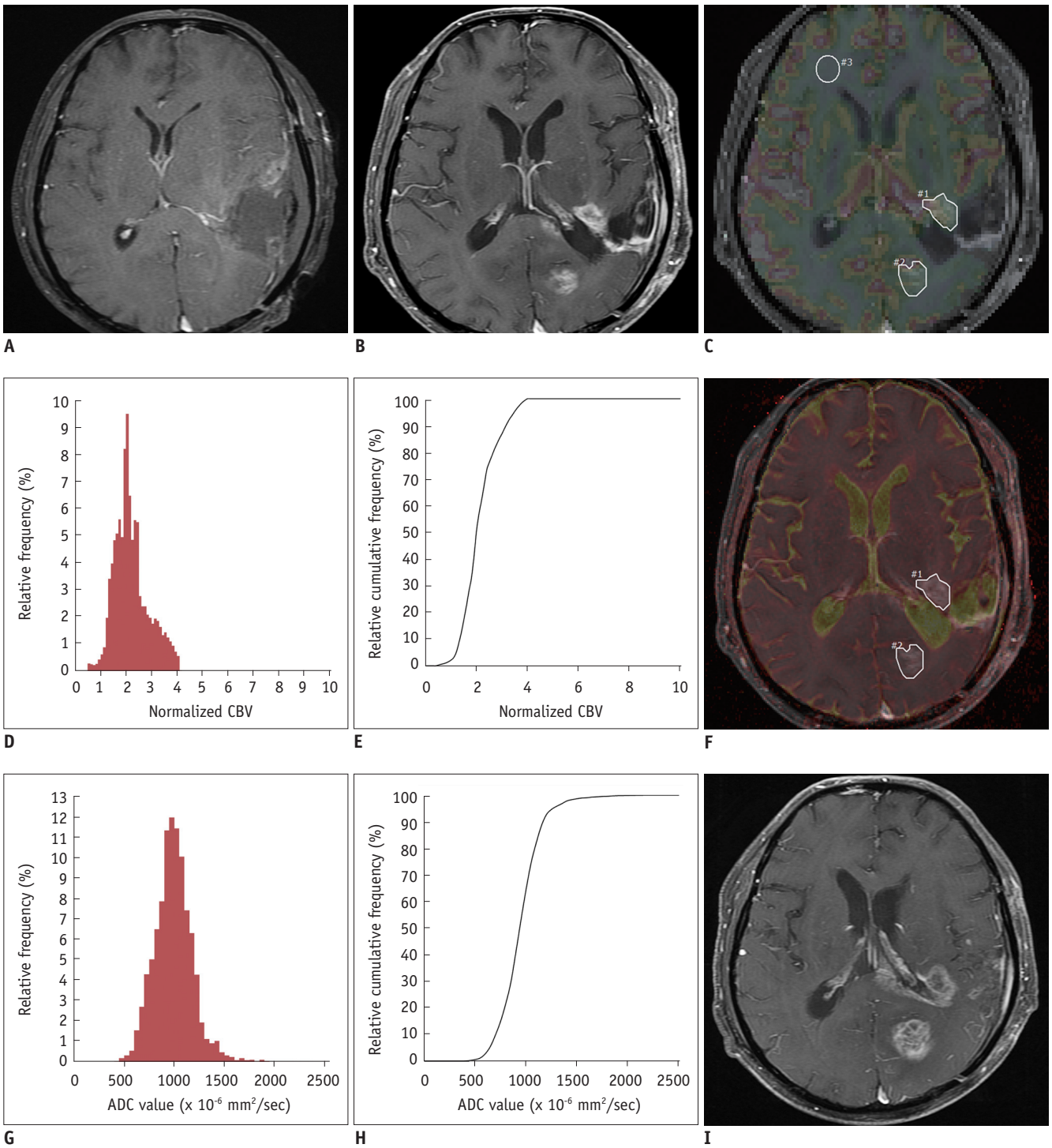

Fig. 2. MR images, nCBV histograms and ADC histograms in 59-year-old man with glioblastoma.
A. Axial CE T1W image taken immediately after gross total resection shows no definite enhancing lesion. **B.** Three weeks after CCRT with TMZ, new enhancing lesions are visible in left periventricular white matter and in left occipital lobe. **C.** nCBV map, which is displayed as color overlay on CE T1W image taken 3 weeks after CCRT with TMZ, shows slightly increased nCBV in lesion (polygonal ROIs #1 and #2) compared with contralateral white matter (round ROI #3). **D.** Normalized CBV histograms and (**E**) cumulative histograms of enhancing lesions. **F.** ADC map, which is displayed as color overlay (in hot scale) on CE T1W image, shows slightly decreased ADC value for lesion (polygonal ROIs #1 and #2). **G.** ADC histograms and (**H**) cumulative histograms of enhancing lesion. **I.** After continuing TMZ for 1 month, patient visited emergency room due to involuntary movement. On second follow-up MR imaging that was performed during visit to emergency room, there was increase in enhancement of lesions without further treatment. After 3 months, patient passed away in spite of continuation of adjuvant TMZ, which is compatible with true progression. ADC = apparent diffusion coefficient, CBV = cerebral blood volume, CCRT = concurrent chemoradiotherapy, CE = contrast-enhanced, nCBV = normalized CBV, ROIs = regions of interest, TMZ = temozolomide, T1W = T1-weighted

Korean Journal of Radiology
KJR

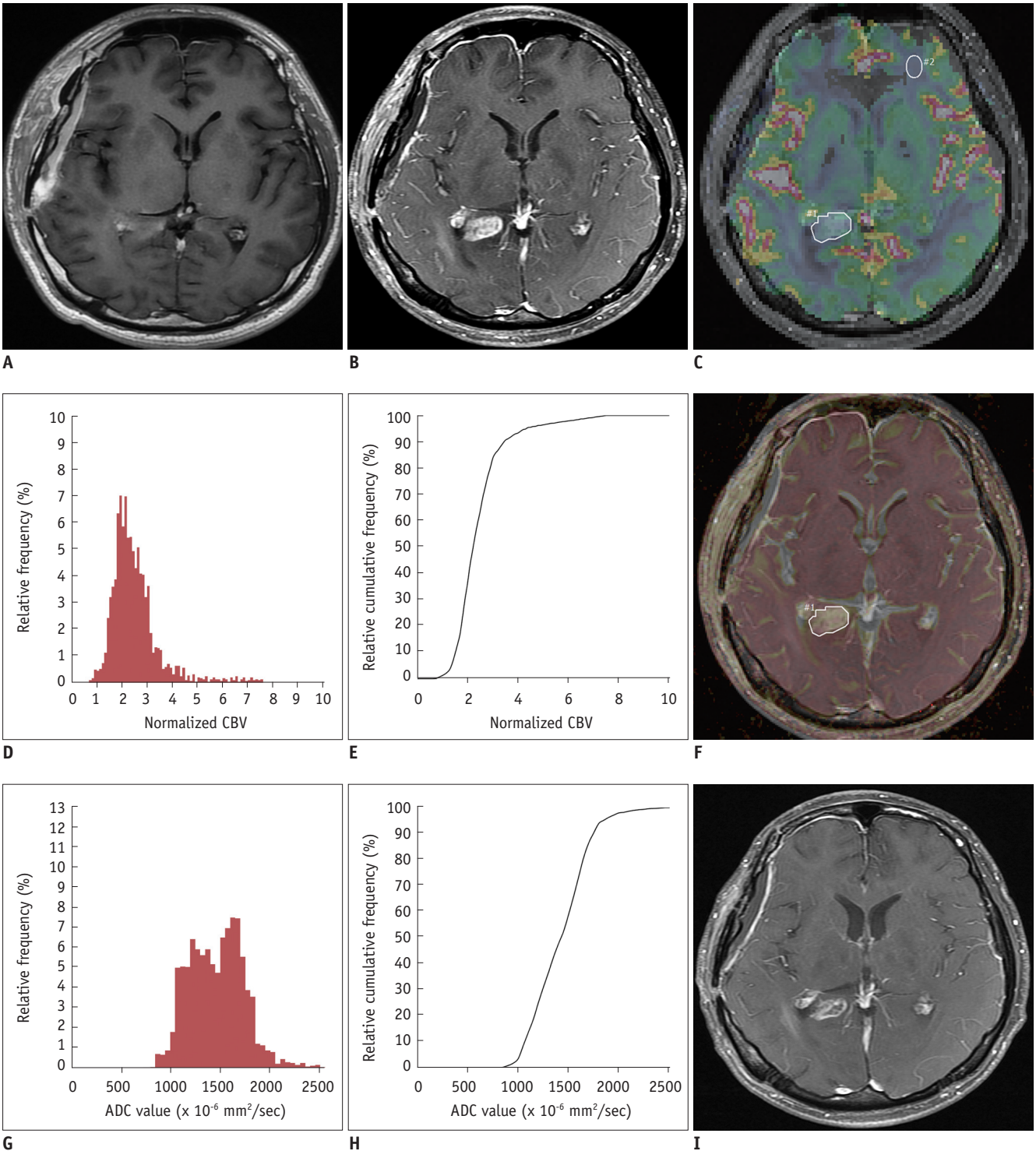

Fig. 3. MR images, nCBV histograms and ADC histograms in 23-year-old man with glioblastoma.
A. Axial CE T1W image taken immediately after gross total resection shows subtle enhancing lesion at right splenium of corpus callosum and (**B**) enlargement of enhancing lesion, 1 month after CCRT with TMZ. **C.** nCBV map, which is displayed as color overlay on CE T1W image taken one month after CCRT with TMZ, shows slightly increased nCBV in lesion (polygonal ROI #1) compared with contralateral white matter (round ROI #2). **D.** Normalized CBV histograms and (**E**) cumulative histograms of enhancing lesion. **F.** ADC map, which is displayed as color overlay (in hot scale) on CE T1W image, shows increased ADC value for lesion (polygonal ROI #1). **G.** ADC histograms and (**H**) cumulative histograms of enhancing lesion. **I.** On second follow-up MR imaging that was performed during outpatient visit after continuing TMZ for 3 months, enhancement of lesion was decreased without further treatment, which confirms pseudoprogression. ADC = apparent diffusion coefficient, CBV = cerebral blood volume, CCRT = concurrent chemoradiotherapy, CE = contrast-enhanced, nCBV = normalized CBV, ROI = region of interest, TMZ = temozolomide, T1W = T1-weighted

two months after CCRT with TMZ. Our results suggest that the lower end values (C5) of the cumulative ADC histograms based on newly visible, entirely enhancing lesions could help in the differentiation of true progression from pseudoprogression.

Because DWI reflects water mobility that is influenced by cellularity, the ADC values are higher in cystic or necrotic areas than in solid tumor components (31, 32). In several studies (12-14, 18), recurrent tumors have shown significantly lower ADC values than those in radiation necrosis, which is possibly due to the differences in cellularity. In this study, the mean ADC had a limited role in the differentiation of true progression from pseudoprogression; however, the C5 of the cumulative ADC histograms was useful in the discrimination between true progression and pseudoprogression. The discordance between the mean ADC and the C5 can be explained by the fact that in true progression there are more cellular components in the newly visible, enhancing lesions after CCRT with TMZ compared to those in pseudoprogression, although both lesions were comosed of both viable tumors and post-CCRT necrosis (11, 17). Thus, the C5 of the cumulative ADC histograms may be more sensitive in predicting true progression because the high cellular portion of the enhancing lesion after CCRT with TMZ may be responsible for the further increase of the enhancing lesion. Our results are consistent with those of a previous study, in which the C5 of the ADC cumulative histogram was the most promising parameter for the preoperative differentiation of high-from low-grade gliomas (24).

The increased contrast enhancement observed in pseudoprogression is considered to represent the effect of treatment on the vasculature, which leads to transient vasodilation, increased vessel permeability, and local inflammation (6, 33). In contrast, one of the essential histopathological features of progression in high-grade glioma is angiogenesis, which is manifested by an elevated tumor vasculature density (34, 35). The CBV is believed to reflect angiogenesis (19, 36). Based on this perspective, several reports have studied the differentiation between recurrent GBM and radiation necrosis (15, 16, 22). Investigators have used histogram parameters such as the mean, maximum, minimum values and the PH, which seem to be useful in discriminating true progression from pseudoprogression. However, in our study, the CBV histogram parameters could not differentiate true progression from pseudoprogression. Similar to our results, Sugahara et al. (19) has previously reported on the overlap in the nCBV values between recurrent primary glial brain tumors and radiation necrosis. We speculate that the limited use of nCBV in our study may be due to the histopathological heterogeneity of the enhancing lesions as well as the inherent limitations associated with nCBV measurements in the vasculature with a disrupted blood-brain barrier (27, 37, 38). Moreover, with respect to CBV measurements, radiation-related transient vasodilation may not be distinguished adequately from angiogenesis within a residual tumor (35, 38).

Apart from the intrinsic limitations of any retrospective study, several other limitations of our study need to be mentioned. First, we used two different 3T MRI scanners with slightly different scan parameters. However, we optimized the sequences to decrease the difference in image quality between the two scanners and used the nCBV value instead of the rCBV value to minimize the effects of different type of MRI scanners or differences in the scan parameters. Nevertheless, we believe that there might be a slight bias in terms of image analysis of the ADC and nCBV maps. Second, there were two patients in the true progression group who were being treated with steroids at the time of the first follow-up MR imaging. Steroid administration in these patients may have influenced the differences in the nCBV or ADC values between the true progression group and the pseudoprogression group (22, 39). Third, this study included a relatively small number of patients. Although we could not find statistical significance regarding the nCBV values between the true progression group and the pseudoprogression group, there is a possibility that a small sample size could have caused negative results on histogram analysis of nCBV. Therefore, further studies with a larger sample size are warranted to verify and strengthen the statistical power of our findings.

In conclusion, our results suggest that the histogram analysis of ADC maps based on newly visible, entirely enhancing lesions can be a useful, objective diagnostic tool for the differentiation of true progression from pseudoprogression in GBM. The 5th percentile value (C5) of the cumulative ADC histogram obtained at b = 0 and 1000 sec/mm^2 can be a promising parameter for the differentiation of true progression from pseudoprogression.

Acknowledgments

The authors thank So Young Yun for her continuous support with updating and organizing the clinical data.

Korean Journal of Radiology
KJR

REFERENCES

1. Jeon HJ, Kong DS, Park KB, Lee JI, Park K, Kim JH, et al. Clinical outcome of concomitant chemoradiotherapy followed by adjuvant temozolomide therapy for glioblastaomas: single-center experience. *Clin Neurol Neurosurg* 2009;111:679-682
2. Erpolat OP, Akmansu M, Goksel F, Bora H, Yaman E, Büyükberber S. Outcome of newly diagnosed glioblastoma patients treated by radiotherapy plus concomitant and adjuvant temozolomide: a long-term analysis. *Tumori* 2009;95:191-197
3. Stupp R, Mason WP, van den Bent MJ, Weller M, Fisher B, Taphoorn MJ, et al. Radiotherapy plus concomitant and adjuvant temozolomide for glioblastoma. *N Engl J Med* 2005;352:987-996
4. Macdonald DR, Cascino TL, Schold SC Jr, Cairncross JG. Response criteria for phase II studies of supratentorial malignant glioma. *J Clin Oncol* 1990;8:1277-1280
5. Taal W, Brandsma D, de Bruin HG, Bromberg JE, Swaak-Kragten AT, Smitt PA, et al. Incidence of early pseudo-progression in a cohort of malignant glioma patients treated with chemoirradiation with temozolomide. *Cancer* 2008;113:405-410
6. Brandsma D, Stalpers L, Taal W, Sminia P, van den Bent MJ. Clinical features, mechanisms, and management of pseudoprogression in malignant gliomas. *Lancet Oncol* 2008;9:453-461
7. Chaskis C, Neyns B, Michotte A, De Ridder M, Everaert H. Pseudoprogression after radiotherapy with concurrent temozolomide for high-grade glioma: clinical observations and working recommendations. *Surg Neurol* 2009;72:423-428
8. Chamberlain MC. Pseudoprogression in glioblastoma. *J Clin Oncol* 2008;26:4359; author reply 4359-4360
9. Dooms GC, Hecht S, Brant-Zawadzki M, Berthiaume Y, Norman D, Newton TH. Brain radiation lesions: MR imaging. *Radiology* 1986;158:149-155
10. Morris JG, Grattan-Smith P, Panegyres PK, O'Neill P, Soo YS, Langlands AO. Delayed cerebral radiation necrosis. *Q J Med* 1994;87:119-129
11. Wen PY, Macdonald DR, Reardon DA, Cloughesy TF, Sorensen AG, Galanis E, et al. Updated response assessment criteria for high-grade gliomas: response assessment in neuro-oncology working group. *J Clin Oncol* 2010;28:1963-1972
12. Hein PA, Eskey CJ, Dunn JF, Hug EB. Diffusion-weighted imaging in the follow-up of treated high-grade gliomas: tumor recurrence versus radiation injury. *AJNR Am J Neuroradiol* 2004;25:201-209
13. Asao C, Korogi Y, Kitajima M, Hirai T, Baba Y, Makino K, et al. Diffusion-weighted imaging of radiation-induced brain injury for differentiation from tumor recurrence. *AJNR Am J Neuroradiol* 2005;26:1455-1460
14. Matsusue E, Fink JR, Rockhill JK, Ogawa T, Maravilla KR. Distinction between glioma progression and post-radiation change by combined physiologic MR imaging. *Neuroradiology* 2010;52:297-306
15. Barajas RF Jr, Chang JS, Segal MR, Parsa AT, McDermott MW, Berger MS, et al. Differentiation of recurrent glioblastoma multiforme from radiation necrosis after external beam radiation therapy with dynamic susceptibility-weighted contrast-enhanced perfusion MR imaging. *Radiology* 2009;253:486-496
16. Hu LS, Baxter LC, Smith KA, Feuerstein BG, Karis JP, Eschbacher JM, et al. Relative cerebral blood volume values to differentiate high-grade glioma recurrence from posttreatment radiation effect: direct correlation between image-guided tissue histopathology and localized dynamic susceptibility-weighted contrast-enhanced perfusion MR imaging measurements. *AJNR Am J Neuroradiol* 2009;30:552-558
17. Kong DS, Kim ST, Kim EH, Lim DH, Kim WS, Suh YL, et al. Diagnostic dilemma of pseudoprogression in the treatment of newly diagnosed glioblastomas: the role of assessing relative cerebral blood flow volume and oxygen-6-methylguanine-DNA methyltransferase promoter methylation status. *AJNR Am J Neuroradiol* 2011;32:382-387
18. Zeng QS, Li CF, Liu H, Zhen JH, Feng DC. Distinction between recurrent glioma and radiation injury using magnetic resonance spectroscopy in combination with diffusion-weighted imaging. *Int J Radiat Oncol Biol Phys* 2007;68:151-158
19. Sugahara T, Korogi Y, Tomiguchi S, Shigematsu Y, Ikushima I, Kira T, et al. Posttherapeutic intraaxial brain tumor: the value of perfusion-sensitive contrast-enhanced MR imaging for differentiating tumor recurrence from nonneoplastic contrast-enhancing tissue. *AJNR Am J Neuroradiol* 2000;21:901-909
20. Pope WB, Lai A, Mehta R, Kim HJ, Qiao J, Young JR, et al. Apparent diffusion coefficient histogram analysis stratifies progression-free survival in newly diagnosed bevacizumab-treated glioblastoma. *AJNR Am J Neuroradiol* 2011;32:882-889
21. Pope WB, Kim HJ, Huo J, Alger J, Brown MS, Gjertson D, et al. Recurrent glioblastoma multiforme: ADC histogram analysis predicts response to bevacizumab treatment. *Radiology* 2009;252:182-189
22. Kim HS, Kim JH, Kim SH, Cho KG, Kim SY. Posttreatment high-grade glioma: usefulness of peak height position with semiquantitative MR perfusion histogram analysis in an entire contrast-enhanced lesion for predicting volume fraction of recurrence. *Radiology* 2010;256:906-915
23. Baek HJ, Kim HS, Kim N, Choi YJ, Kim YJ. Percent change of perfusion skewness and kurtosis: a potential imaging biomarker for early treatment response in patients with newly diagnosed glioblastomas. *Radiology* 2012;264:834-843
24. Kang Y, Choi SH, Kim YJ, Kim KG, Sohn CH, Kim JH, et al. Gliomas: histogram analysis of apparent diffusion coefficient maps with standard- or high-b-value diffusion-weighted MR imaging--correlation with tumor grade. *Radiology* 2011;261:882-890
25. Rosen BR, Belliveau JW, Vevea JM, Brady TJ. Perfusion

imaging with NMR contrast agents. *Magn Reson Med* 1990;14:249-265
26. Ostergaard L, Weisskoff RM, Chesler DA, Gyldensted C, Rosen BR. High resolution measurement of cerebral blood flow using intravascular tracer bolus passages. Part I: mathematical approach and statistical analysis. *Magn Reson Med* 1996;36:715-725
27. Boxerman JL, Schmainda KM, Weisskoff RM. Relative cerebral blood volume maps corrected for contrast agent extravasation significantly correlate with glioma tumor grade, whereas uncorrected maps do not. *AJNR Am J Neuroradiol* 2006;27:859-867
28. Wetzel SG, Cha S, Johnson G, Lee P, Law M, Kasow DL, et al. Relative cerebral blood volume measurements in intracranial mass lesions: interobserver and intraobserver reproducibility study. *Radiology* 2002;224:797-803
29. Bjornerud A. The ICE software package: direct co-registration of anatomical and functional datasets using DICOM image geometry information. *Proc Hum Brain Mapping* 2003;19:1018p
30. Tozer DJ, Jäger HR, Danchaivijitr N, Benton CE, Tofts PS, Rees JH, et al. Apparent diffusion coefficient histograms may predict low-grade glioma subtype. *NMR Biomed* 2007;20:49-57
31. Padhani AR, Liu G, Koh DM, Chenevert TL, Thoeny HC, Takahara T, et al. Diffusion-weighted magnetic resonance imaging as a cancer biomarker: consensus and recommendations. *Neoplasia* 2009;11:102-125
32. Sugahara T, Korogi Y, Kochi M, Ikushima I, Shigematu Y, Hirai T, et al. Usefulness of diffusion-weighted MRI with echo-planar technique in the evaluation of cellularity in gliomas. *J Magn Reson Imaging* 1999;9:53-60
33. de Wit MC, de Bruin HG, Eijkenboom W, Sillevis Smitt PA, van den Bent MJ. Immediate post-radiotherapy changes in malignant glioma can mimic tumor progression. *Neurology* 2004;63:535-537
34. Oh BC, Pagnini PG, Wang MY, Liu CY, Kim PE, Yu C, et al. Stereotactic radiosurgery: adjacent tissue injury and response after high-dose single fraction radiation: Part I--Histology, imaging, and molecular events. *Neurosurgery* 2007;60:31-44; discussion 44-45
35. Wesseling P, Ruiter DJ, Burger PC. Angiogenesis in brain tumors; pathobiological and clinical aspects. *J Neurooncol* 1997;32:253-265
36. Cha S, Knopp EA, Johnson G, Litt A, Glass J, Gruber ML, et al. Dynamic contrast-enhanced T2-weighted MR imaging of recurrent malignant gliomas treated with thalidomide and carboplatin. *AJNR Am J Neuroradiol* 2000;21:881-890
37. Heiland S, Benner T, Debus J, Rempp K, Reith W, Sartor K. Simultaneous assessment of cerebral hemodynamics and contrast agent uptake in lesions with disrupted blood-brain-barrier. *Magn Reson Imaging* 1999;17:21-27
38. Spiegelmann R, Friedman WA, Bova FJ, Theele DP, Mickle JP. LINAC radiosurgery: an animal model. *J Neurosurg* 1993;78:638-644
39. Minamikawa S, Kono K, Nakayama K, Yokote H, Tashiro T, Nishio A, et al. Glucocorticoid treatment of brain tumor patients: changes of apparent diffusion coefficient values measured by MR diffusion imaging. *Neuroradiology* 2004;46:805-811